

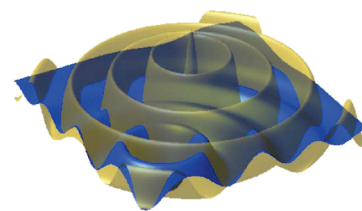
X-ray Spectroscopic Measurement of Photoelectron Inelastic Mean Free Paths in Molybdenum

Christopher T. Chantler* and Jay D. Bourke

School of Physics, University of Melbourne, Parkville, VIC, 3010 Australia

ABSTRACT The electron inelastic mean free path (IMFP) of molybdenum is determined experimentally over an energy range of 1–120 eV using analysis of X-ray absorption fine structure (XAFS). This new approach enables accurate measurements of IMFPs in this energy range where direct measurements are often difficult and highly uncertain, and provides a means for studying materials inaccessible through current alternate techniques. This approach can also be used to determine localized IMFPs within complex molecular systems, enabling detailed study of surfaces and nanoenvironments. This information is important for diverse applications in physical chemistry including electron microscopy, spectroscopy, and diffraction (low-energy electron diffraction (LEED) and electron energy loss spectroscopy (EELS) in particular). Here we reveal the accuracy achievable using experimental data of high statistical precision, and critically evaluate the form of the IMFP in the asymptotic region in the low energy limit.

SECTION Electron Transport, Optical and Electronic Devices, Hard Matter



The electron inelastic mean free path (IMFP) is the average distance traveled between successive inelastic collisions for an electron moving with a particular energy in a given material.¹ It is a parameter of fundamental importance to a range of fields including electron microscopy,² auger electron spectroscopy,³ X-ray photoelectron spectroscopy,⁴ photoelectron diffraction,⁵ and many others (Figure 1). Comprehensive tabulations of IMFPs have been published spanning large energy ranges and covering numerous elements and selected compounds.^{6,7}

There are, however, two serious shortcomings in available prescriptions and tabulations. The first is that both experimental and theoretical IMFPs in the low energy region, below 200 eV, are commonly unavailable, and when available show significant variation between approaches.⁸ The second is that the IMFPs of many materials are inaccessible by established experimental approaches, and equally by much of the current theory due to its reliance on experimental optical data.⁹ Common experiments involving low-energy electron diffraction (LEED)¹⁰ or photoelectron spectroscopy can directly measure the attenuation length, but can be unsuitable for bulk IMFP determination due to elastic contamination and surface effects.¹¹

Our work focuses on a new technique that uses analysis of X-ray absorption fine structure (XAFS) measurements. This method provides an approach uniquely suited to the low-energy regime. In addition, the scope of materials for which measurements can be made with our approach is almost limitless, and potentially includes even embedded nanostructures. We use the sensitivity of near-edge XAFS (often called XANES) to the finite lifetime of the photoelectron to match our well-defined theoretical predictions to high-accuracy XAFS measurements.

XAFS refers to the small, rapidly oscillating components of the photoelectric absorption curve of a material that typically appear at energies within a few hundred electron volts above an absorption edge. This structure is formed by interference of the photoelectron wave function as it is backscattered by surrounding atomic cores. It is highly sensitive to bond lengths and co-ordination numbers, in addition to thermal vibrations and the photoelectron energy. The relatively short lifetime of the photoelectron at low energies causes an energy uncertainty and subsequent smearing of the XAFS curve, which is observable and quantifiable given high precision measurements.

The effect of the finite IMFP can be visualized by considering an exponential reduction in the outgoing and returning photoelectron wave function, as shown stylistically in Figure 2. Figure 2A illustrates a situation where an infinite IMFP leads to no reduction in the returning wave function at the core of the absorbing atom. In Figure 2B, a finite IMFP yields a reduction with the effect of diminishing the level of interference (coherence) between the outgoing (yellow/lightly colored) and returning (blue/dark colored) waves. Due to a Fourier relationship between the reflected wave function and the resulting XAFS spectrum, this exponential damping leads to a broadening of the XAFS peaks, with corresponding energy uncertainty. This effect is strongest below 100–200 eV, where the amplitude of the XAFS oscillations is high, and is quantified by the photoelectron lifetime, or IMFP.

Received Date: June 8, 2010

Accepted Date: July 15, 2010

Published on Web Date: July 26, 2010

Our extraction of the IMFP from experimental XAFS data requires a robust theoretical model for XAFS calculations. We use the finite difference method (FDM), a development of the finite difference method for near-edge structure (FDMNES) first implemented by Joly.¹² This approach determines the absorption cross section using excited state wave functions calculated over a finite grid spanning a small ($r < 8 \text{ \AA}$) cluster of atoms. This approach is favored due to its accurate representation of atomic potentials and applicability to complex molecular structures.¹³ For this work, we use FDM to calculate

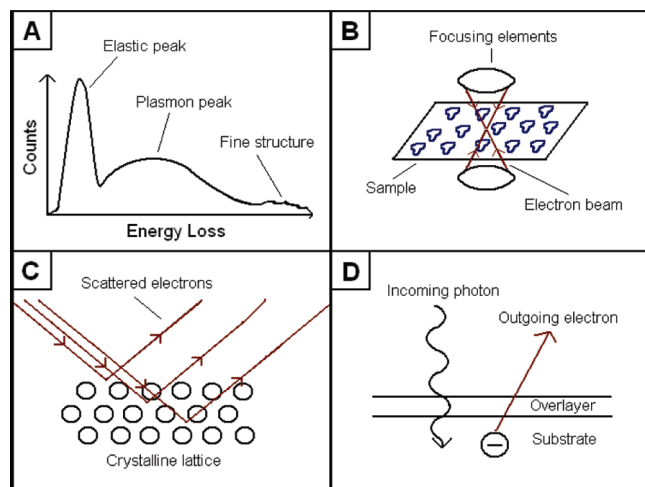


Figure 1. Schematics of fields in which knowledge of the electron IMFP is important. (A) Stylized electron energy loss spectroscopy (EELS) spectrum; (B) schematic of a transmission electron microscope (TEM); (C) Electron diffraction experiment. (D) Overlayer film technique, a useful experimental approach at higher energies. Our work aims to provide a substantial correction to theoretical, semiempirical, and alternate experimental extrapolation for these fields, especially in low energy measurements, and expands the types of materials for which an IMFP can be investigated.

the absorption spectrum for molybdenum up to 200 eV from the K absorption edge. The critical part of the absorption spectrum is the oscillatory component $\chi(E)$, given by

$$\chi(E) = \frac{\mu(E)}{\mu(E)_0} - 1 \quad (1)$$

where $\mu(E)$ and $\mu(E)_0$ are the total solid-state absorption, and atomic (or atom-like) absorption coefficients, respectively. The oscillatory component of the theoretical absorption curve is matched with its experimental counterpart following a complex processing and fitting algorithm. In addition to the effects of inelastic losses (i.e., via the IMFP), processes such as thermal vibration and core-hole relaxation are incorporated through well-known parameters.

Figure 3 illustrates the relative magnitude of these effects on the oscillatory component of the calculated XAFS. The inelastic losses are quantified through our fitted values for the IMFP. The theoretical predictions achieve excellent agreement with experiment for the entire range shown, and the strong influence of inelastic losses is apparent below 100 eV. Error bars of the experimental data are too small to plot on this scale, but include both statistical precision and all known sources of uncertainty in accuracy.

The IMFP contribution is represented by an energy-dependent Lorentzian broadening of width $\Gamma(E)$. Figure 4 shows the width determined by our fitting and processing algorithm with three standard error uncertainty. For comparison, widths are shown using IMFP data taken from the theoretical calculation of Tanuma et al.⁶ and the experimental measurements of Lesiak et al.¹⁴

These widths transform directly to the IMFP, but are mostly significant in terms of consequent energy resolution in the X-ray fine structure. Probing crystal structure around a central absorber using photoelectrons has a natural radial limitation, as distant atomic cores will not be reached by electrons with

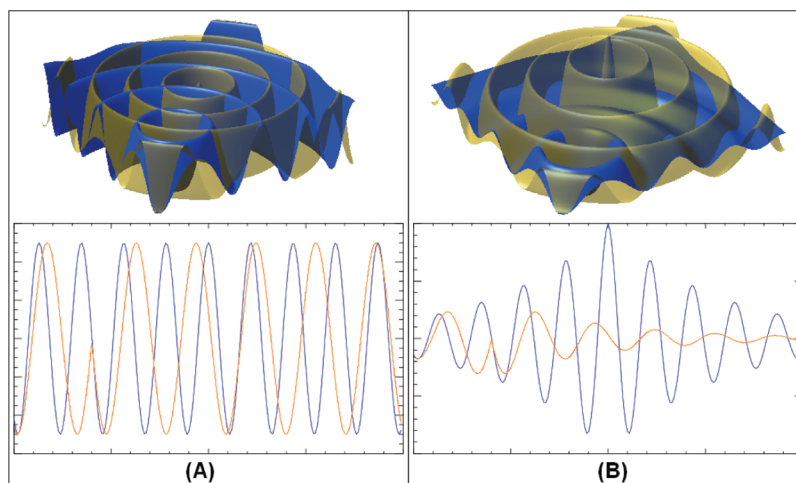


Figure 2. Stylized two- and one-dimensional views of electron wave functions emitted by a central atom (yellow/lightly colored wave) before being backscattered by a surrounding atom (blue/dark wave). The interference between the two at the point of the central atom causes the complex oscillations seen in XAFS. Panel A shows this situation in the case where the electron IMFP is assumed infinite, while for B this value is finite, reducing the amplitude of the backscattered wave. Note the significant impact on the level of interference, and therefore on the resulting XAFS spectrum.

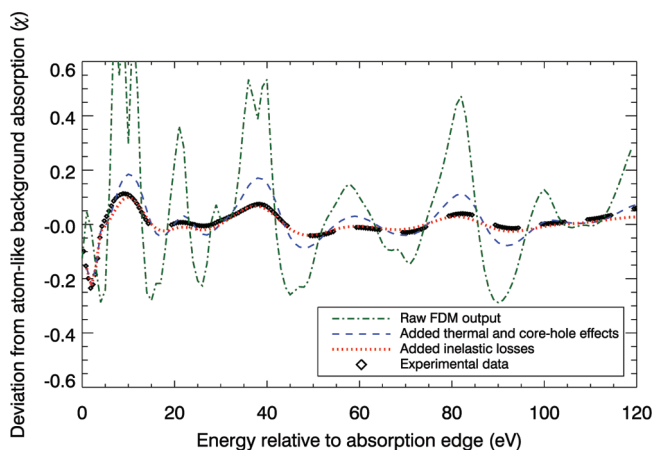


Figure 3. Relative effects of different processes on the oscillatory component of the determined XAFS of molybdenum. Thermal effects are quantified through a Debye–Waller-dependent damping of the oscillations, while the core–hole relaxation produces a static 5.87 eV Lorentzian convolution with fitted width related directly to the electron IMFP. The experimental data are measured on an absolute scale, and the corresponding small error bars, less than the line width, are the accuracy of the result.

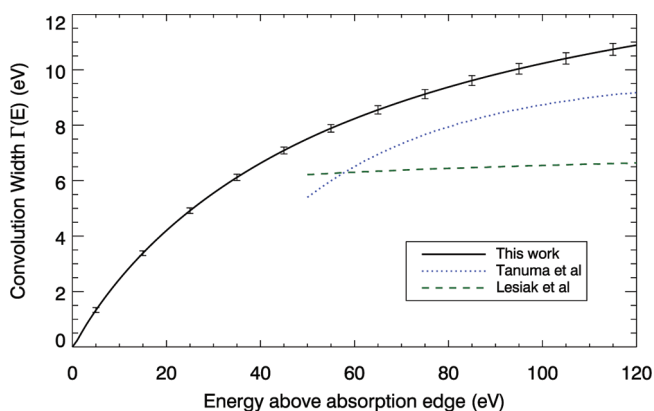


Figure 4. Width of the Lorentzian $\Gamma(E)$ accounting for the effect of the finite IMFP, with three standard deviation uncertainty plotted. This curve is produced by fitting the resultant convolved spectrum with the experimental data of de Jonge et al.,¹⁵ using an implementation of the Levenberg–Marquardt least-squares fitting procedure. Also shown are the convolution widths corresponding to measurements of the IMFP by Lesiak et al.,¹⁴ and theoretical values from Tanuma et al.⁶

short IMFPs. Comparison with the resultant IMFP measurements in Figure 5 demonstrates further, however, that even for energies above 100 eV where the IMFP is increasing, the Lorentzian broadening is also increasing. This means that distant cores, which produce narrow fine structure, are being increasingly filtered at higher energies despite a greater range of photoelectron coherence. Effectively, as the energy increases, we are probing an ever smaller region around the central absorbing atom, with an expected limiting behavior of the absorption curve reducing to that of an isolated atom. Consequently, we are sensitive to an increasingly localized IMFP, which may vary considerably from the bulk IMFP in complex molecules.

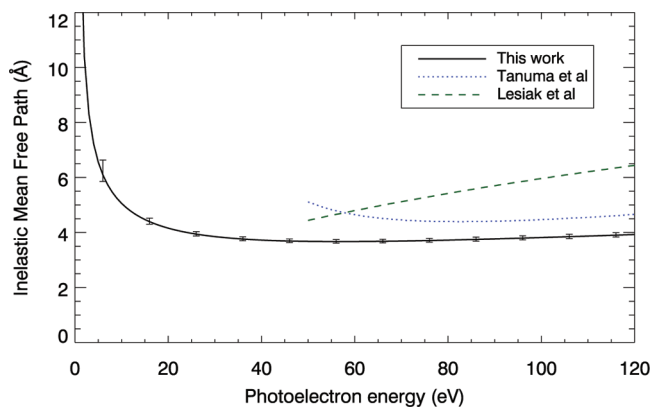


Figure 5. The IMFP for molybdenum as determined from XAFS measurements, with three standard deviation error bars. Also shown is a theoretical calculation from Tanuma et al.⁶ and measurements from Lesiak et al.¹⁴

Figure 5 illustrates the determined IMFP of elemental molybdenum, in comparison with corresponding predictions of Tanuma et al. and data from Lesiak et al. Although relatively few theoretical studies have been conducted on molybdenum, Tanuma et al. are usually consistent with others for the materials they have studied. As discussed later, the optical data model on which their work is based is widely employed.

Lesiak et al. have made measurements using elastic peak electron spectroscopy (EPES). In this technique, electrons of well-defined energy are incident on a smooth solid surface, and the relative intensity of the elastically scattered signal is measured. This signal is compared with that of a Ni reference solid of known IMFP, while corrections are made for multiple elastic scattering events via a Monte Carlo calculation. Naturally the accuracy of the reference IMFP and the details of the Monte Carlo calculation are strong determinants of the applicability of this approach, and variations of up to 20% between different measurements are common.

Our results show a significant decrease in IMFP from alternative approaches. The low-energy extrapolation of Lesiak et al may have shown greater consistency; however, this is impractical given the shape of the curve. In addition, corrections for surface excitations in the EPES measurement may have been significant, particularly where the IMFP is low. We see qualitative agreement with the form given by Tanuma et al., increasingly at higher energies where their theory is expected to be more applicable. An investigation of copper also predicted lower IMFPs than are typical in the literature at energies below 100 eV.⁸

This work not only demonstrates a new method of experimental IMFP determination, but has the potential to act as a strong discriminator between alternate theoretical approaches. Although reliable IMFPs are extensively tabulated at kiloelectron volt energies, the behavior of the IMFP below 200 eV is strongly dependent on the approach used.⁸

Most IMFP calculations use a variation of the optical data model of Penn,⁹ which requires first a determination of the optical dielectric function, and second an extension of this data into the realm of finite momentum transfer. The optical data can be taken from experiments¹⁶ or band structure calculations.¹⁷

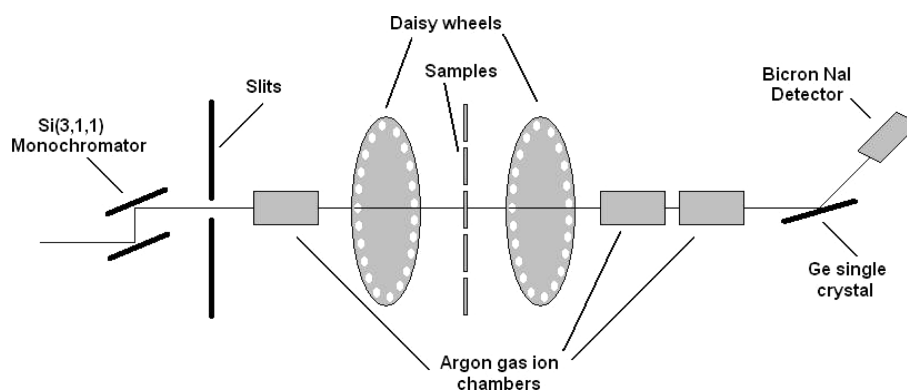


Figure 6. Schematic of the experimental setup used to measure XAFS. Synchrotron radiation is monochromated and collimated before passing through an argon gas ion chamber detector, and then striking the sample foil. The outgoing radiation is detected by two further ion chambers, while energy measurements are made via diffraction onto a NaI scintillation detector. Daisy wheels are located on either side of the sample, containing beam-attenuating foils for quantification of harmonic contamination.

Tanuma et al. used experimental data that had been tested for self-consistency with the use of sum-rules. The extension to finite momentum transfer can be done in a variety of ways, the most popular being the Penn approach used by Tanuma et al.⁶ and the Drude-type representation favored by Kwei et al.¹⁸ Typical IMFP variations are conservatively estimated as 10% at 100 eV, 50% at 50 eV, and any arbitrary amount at 10 eV.

Denton et al. report the use of these techniques in addition to a third using Mermin-type terms, which explicitly include broadening effects at finite momentum transfer.¹⁹ Despite focusing on different materials (in this case, elemental Al and Au), this work reveals dramatic differences between alternate approaches at low energies. It is exciting to consider that our new experimental approach may be integral in critically evaluating these theoretical models.

Our determined IMFP of molybdenum is also unique in that it retains precision, even well below the energy corresponding to the broad minimum and into the asymptotic region at the low energy limit. Such energies are immensely difficult to probe directly. Ballistic electron emission microscopy (BEEM) claims some precision in this region.²⁰ Our increased accuracy here is particularly due to the large number of data points and high-accuracy energy measurements made during the XAFS experiment. This was a painstaking experiment requiring several days of data collection; however, it is an excellent demonstration of what is possible given our most rigorous experimental techniques.

The XAFS approach to IMFP determination has been demonstrated to remain precise at energies as low as a few electron volts. These results form important reference data for a variety of experimental systems, and may be integral in the future evaluation of theoretical models. Further developments and experimentation will enable investigation of not only elemental solids, but potentially many-atom compounds, solutions, polycrystalline materials and mixtures, and may yield position-dependent information in strongly inhomogeneous media.

METHODS

Experimental XAFS data is collected using the X-ray extended range technique (XERT).²¹ Synchrotron radiation

is incident on a double-reflection monochromator, before passing through beam-defining slits, which produce a cross sectional area of approximately 1 mm². Intensity measurements are made using argon gas ion chambers upstream and downstream for improved statistics and the investigation of detector nonlinearities (Figure 6). Two daisy wheels are located between the ion chambers and the sample with a selection of apertures subtending different solid angles. The daisy wheels also have up to 30 foils covering X-ray attenuation over 3 orders of magnitude. This enables quantification of the levels of harmonics and other systematics in the X-ray beam.

The energy of the beam is measured using diffraction from a single germanium crystal onto a stationary sodium iodide scintillation detector. The germanium crystal is rotated through a range of angles around the Bragg angle. The samples consist of foils ranging in thickness from roughly 25 to 250 μm with a cross-sectional area of 25 × 25 mm². Sample impurities contribute less than 0.01% to uncertainties in the X-ray attenuation coefficients. The samples are characterized using a full foil mapping technique to determine surface roughness²² in addition to the integrated column density, and to allow for corrections due to the sample holders.^{23,24}

The IMFP manifests itself in XAFS via a lifetime broadening effect. This effect is explicitly a Lorentzian broadening of the solid-state (i.e., oscillatory) component of the absorption spectrum. This component must therefore be extracted from the total absorption spectrum determined via FDM. The oscillations, commonly denoted $\chi(E)$ and defined in eq 1, are broadened by a Lorentzian function of varying width $\Gamma(E)$, attenuated to account for thermal motion within the cluster,²⁵ and subsequently incorporated into the total absorption spectrum.

This process requires several stages of calculation and data manipulation. First, the total absorption spectrum for solid molybdenum and the absorption spectrum for an isolated molybdenum atom must be calculated using FDM from -10 to 200 eV relative to the K absorption edge. This allows a direct extraction of the oscillatory component of the solid state curve. This component is then broadened by a Lorentzian of

width $\Gamma(E)$ to account for the effects of inelastic losses involving both the IMFP and the core–hole relaxation. It is exponentially damped to represent the effects of thermal motion. The thermal damping uses well-quantified parameters (the temperature- and material-dependent Debye–Waller factor), while the core–hole relaxation width is calculated from transition rates or experimentally observed lifetimes. The energy-dependent part of $\Gamma(E)$ is related to the photoelectron IMFP following:

$$\Gamma(E) = \frac{\hbar}{\lambda(E)} \sqrt{\frac{2E}{m_e}} + \Gamma_H \quad (2)$$

where E is the electron energy and distance from the absorption edge, and $\lambda(E)$ is the IMFP. Γ_H is the material-dependent core–hole relaxation width.

With an initially approximated IMFP, the convolved and damped oscillatory component $\chi(E)$ can be recombined with the atomic absorption $\mu_0(E)$ and compared with experimental measurements, in this case those determined by de Jonge et al.¹⁵ This procedure is done iteratively with fitting parameters $x_0 \dots x_n$ for the convolution width such that

$$\Gamma(E) = \frac{\sum_{i=1}^n E^{nx_0}}{\sum_{i=1}^n \frac{1}{x_i} E^{nx_0}} + \Gamma_H \quad (3)$$

This functional form is chosen to ensure the broadening increases from zero at the absorption edge to a constant value (x_n) at the high energy limit. This is consistent with widths produced using literature values of the IMFP across a range of materials at energies below 150 eV. For this work adequate agreement with experiment is reached using $n = 4$. Three additional fitting parameters are required for the low-energy atomic absorption offset²⁶ and the edge energy offset.

The fitting utilizes a FORTRAN implementation of the Levenberg–Marquardt least-squares method, and can take several minutes, or a few hours for cases with many data points and a complex convolution function. Fitting uncertainties are determined as part of the procedure.

AUTHOR INFORMATION

Corresponding Author:

*To whom correspondence should be addressed. E-mail: chantler@unimelb.edu.au.

ACKNOWLEDGMENT The authors acknowledge the work of Y. Joly and J. L. Glover in our developments with FDMNES, and the work of the experimental teams who measured our high-accuracy XAFS data. We also acknowledge the ASRP for providing the funding for the experimental data used in this research.

REFERENCES

- Powell, C. J.; Jablonski, A. Surface Sensitivity of X-ray Photoelectron Spectroscopy. *Nucl. Instrum. Methods, A* **2009**, *601*, 54–65.
- Kimoto, K.; Asaka, T.; Nagai, T.; Saito, M.; Matsui, Y.; Ishizuka, K. Element-Selective Imaging of Atomic Columns in a Crystal Using STEM and EELS. *Nature* **2007**, *450*, 702–704.
- Werner, W. S. M.; Smekal, W.; Stori, H.; Winter, H.; Stefani, G.; Ruocco, A.; Offi, F.; Gotter, R.; Morgante, A.; Tommasini, F. Emission-Depth-Selective Auger Photoelectron Coincidence Spectroscopy. *Phys. Rev. Lett.* **2005**, *94*, 038302–038305.
- Cumpson, P. J. Elastic Scattering Corrections in AES and XPS. III. Behaviour of Electron Transport Mean Free Path in Solids for Kinetic Energies in the Range 100 eV < E < 400 eV. *Surf. Interface Anal.* **1997**, *25*, 447–453.
- Hillebrecht, F. U.; Rose, H. B.; Kinoshita, T.; Idzerda, Y. U.; van der Laan, G.; Denecke, R.; Ley, L. Photoelectron Diffraction in Magnetic Linear Dichroism. *Phys. Rev. Lett.* **1995**, *75*, 2883–2886.
- Tanuma, S.; Powell, C. J.; Penn, D. R. Calculations of Electron Inelastic Mean Free Paths. II. Data for 27 Elements over the 50–2000 eV Range. *Surf. Interface Anal.* **1991**, *17*, 911–926.
- Tanuma, S.; Powell, C. J.; Penn, D. R. Calculations of Electron Inelastic Mean Free Paths for 31 Materials. *Surf. Interface Anal.* **1988**, *11*, 577–589.
- Bourke, J. D.; Chantler, C. T. Measurements of Electron Inelastic Mean Free Paths in Materials. *Phys. Rev. Lett.* **2010**, *104*, 206601–206604.
- Penn, D. R. Electron Mean-Free-Path Calculations Using a Model Dielectric Function. *Phys. Rev. B* **1987**, *35*, 482–486.
- Rundgren, J. Electron Inelastic Mean Free Path, Electron Attenuation Length, and Low-Energy Electron-Diffraction Theory. *Phys. Rev. B* **1999**, *59*, 5106–5114.
- Lindau, I.; Spicer, W. E. The Probing Depth in Photoemission and Auger-Electron Spectroscopy. *J. Elec. Spectrosc. Rel. Phenom.* **1974**, *3*, 409–413.
- Joly, Y. X-ray Absorption Near-Edge Structure Calculations beyond the Muffin-Tin Approximation. *Phys. Rev. B* **2001**, *63*, 125120–125130.
- Glover, J. L.; Chantler, C. T.; Soldatov, A. V.; Smolentsev, G.; Feiters, M. C. Theoretical XANES Study of the Activated Nickel (*t*-Amylisocyanide) Molecule. *AIP Conf. Proc.* **2007**, *882*, 625–627.
- Lesiak, B.; Jablonski, A.; Zommer, L.; Kosinski, A.; Gergely, G.; Konkol, A.; Sulyok, A.; Daroczi, C. S.; Nagy, P. Comparison of Al and Ni Reference Samples for Determining the Inelastic Mean Free Path of Electrons Using Different Electron Spectrometers. *Proc. ECASIA95* **1996**, 619–622.
- de Jonge, M. D.; Tran, C. Q.; Chantler, C. T.; Barnea, Z.; Dhal, B. B.; Cookson, D. J.; Lee, W.; Mashayekhi, A. Measurement of the X-ray Mass Attenuation Coefficient and Determination of the Imaginary Component of the Atomic Form Factor of Molybdenum over the 13.5–41.5-keV Energy Range. *Phys. Rev. A* **2005**, *71*, 032702–032717.
- Ding, Z.-J.; Shimizu, R. Inelastic Collisions of kV Electrons in Solids. *Surf. Sci.* **1989**, *222*, 313–351.
- Sorini, A. P.; Kas, J. J.; Rehr, J. J.; Prange, M. P.; Levine, Z. H. Ab Initio Calculations of Electron Inelastic Mean Free Paths and Stopping Powers. *Phys. Rev. B* **2008**, *74*, 165111–165118.
- Kwei, C. M.; Chen, Y. F.; Tung, C. J.; Wang, J. P. Electron Inelastic Mean Free Paths for Plasmon Excitations and Interband Transitions. *Surf. Sci.* **1993**, *293*, 202–210.
- Denton, C. D.; Abril, I.; Garcia-Molina, R.; Moreno-Marin, J. C.; Heredia-Avalos, S. Influence of the Description of the Target Energy-Loss Function on the Energy Loss of Swift Projectiles. *Surf. Interface Anal.* **2008**, *40*, 1481–1487.
- Lu, R. P.; Morgan, B. A.; Kavanagh, K. L.; Powell, C. J.; Chen, P. J.; Serpa, F. G.; Egelhoff, W. F., Jr. Hot-Electron Attenuation Lengths in Ultrathin Magnetic Films. *J. Appl. Phys.* **2000**, *87*, 5164–5166.

- (21) Chantler, C. T. Development and Applications of Accurate Measurement of X-ray Absorption. *Eur. Phys. J. Spec. Top.* **2009**, *169*, 147–153.
- (22) Glover, J. L.; Chantler, C. T.; de Jonge, M. D. Nano-roughness in Gold Revealed from X-ray Signature. *Phys. Lett. A* **2009**, *373*, 1177–1180.
- (23) Rae, N. A.; Glover, J. L.; Chantler, C. T. An Improvement to the Full-Foil Mapping Technique for High Accuracy Measurement of X-ray Mass Attenuation Coefficients. *Nucl. Instrum. Methods, A* **2010**, *619*, 47–50.
- (24) de Jonge, M. D.; Barnea, Z.; Tran, C. Q.; Chantler, C. T. Full-Foil Mapping of Integrated Column Density Applied to the Absolute Determination of the Mass Attenuation Coefficients. *Meas. Sci. Technol.* **2004**, *15*, 1811–1822.
- (25) Bourke, J. D.; Chantler, C. T.; Witte, C. Finite Difference Method Calculations of X-ray Absorption Fine Structure for Copper. *Phys. Lett. A* **2007**, *360*, 702–706.
- (26) Bourke, J. D.; Chantler, C. T. Finite Difference Method Calculations of Long-Range X-ray Absorption Fine Structure for Copper over k 20A-1. *Nucl. Instrum. Methods, A* **2010**, *619*, 33–36.